
Efficient Sampling-Based Bayesian Active Learning

Camille Gontier

Department of Physiology
University of Bern
camille.gontier@unibe.ch

Simone Carlo Surace

Department of Physiology
University of Bern
simone.surace@unibe.ch

Igor Delvendahl

Department of Molecular Life Sciences
Neuroscience Center Zurich
University of Zurich
igor.delvendahl@uzh.ch

Martin Müller

Department of Molecular Life Sciences
Neuroscience Center Zurich
University of Zurich
martin.mueller@mls.uzh.ch

Jean-Pascal Pfister

Department of Physiology
University of Bern
jeanpascal.pfister@unibe.ch

Abstract

Bayesian Active Learning (BAL) is an efficient framework for learning the parameters of a model, in which input stimuli are selected to maximize the mutual information between the observations and the unknown parameters. However, its applicability to real experiments is limited by two main drawbacks. Firstly, it requires performing high-dimensional integrations and optimizations in real time: current methods are either too time consuming, or only applicable to specific models. Secondly, it only optimizes for the next stimulus input (an approach referred to as a myopic design), disregarding all future observations in the experiment. To address these issues, we propose an Efficient Sampling-Based Bayesian Active Learning (ESB-BAL) framework, which is efficient enough to be used in real-time biological experiments and to go beyond myopic approaches. We apply our method to the problem of estimating the parameters of a chemical synapse from its postsynaptic responses evoked by presynaptic action potentials. Synaptic parameter inference is a challenging application of BAL, as computation needs to be faster than the smallest inter-stimulation interval, which can be on the order of a few milliseconds. Using synthetic data and synaptic whole-cell patch clamp recordings in cerebellar brain slices, we show that our method has the potential to significantly improve the precision of model-based inferences, thereby paving the way towards more systematic and automated experimental designs.

1 Introduction

In machine learning, a central problem is that of inferring the parameters θ of a model \mathcal{M} . For instance, in supervised learning, one may want to learn the parameters of a Deep Neural Network (DNN) so as to minimize the difference between its output and training labels; in biology, the parameters of a system can be studied by fitting a biophysical model to recorded observations. In most cases, these parameters can be neither directly measured nor analytically computed, but can be inferred using the recorded outputs of the system \mathbf{x} as a response to input stimuli Ψ . By computing the

likelihood of the outputs given the inputs and the parameters $p(\mathbf{x}|\Psi, \theta)$, it is possible to obtain either a point-based estimate of the parameters $\arg \max_{\theta} p(\mathbf{x}|\Psi, \theta)$ [1], or to use the Metropolis-Hastings (MH) algorithm to compute their full posterior distribution $p(\theta|\mathbf{x}, \Psi) \propto p(\mathbf{x}|\Psi, \theta)$ [2].

However, the accuracy of these estimates critically depends on the pair (Ψ, \mathbf{x}) , and especially on how the input stimuli are chosen. For instance, training a DNN on non-i.i.d. training examples (i.e. blocked training) will lead to catastrophic forgetting [3]. In biology, most experiments still rely on pre-defined and non-adaptive protocols Ψ , which may not yield sufficient information about the true parameters of the studied system. As a consequence, those experiments require more observations, which increases their cost, time, and need for subjects. An efficient framework to alleviate this issue is called Bayesian Active Learning (BAL). Knowing the current estimate of the parameters, the experimental protocol (i.e. the next input) can be optimized on the fly so as to maximize the mutual information between the recordings and the parameters (Figure 1 (a)). BAL is a branch of Optimal Experiment Design (OED) theory [4, 5, 6]. It has already been used in neuroscience to infer the parameters of a Generalized Linear Model (GLM) [7], the receptive field of a neuron [8], or the nonlinearity in a linear-nonlinear-Poisson (LNP) encoding model [9]. Implementing BAL for biological settings can be challenging, especially for real-time applications: it requires computing an update of the posterior distribution of parameters after each time step, and using it to compute the expected information gain from future experiments, which involves solving an optimization problem over a possibly high-dimensional stimulus space.

Our main contribution is to provide a general framework for online active learning, called Efficient Sampling-Based Bayesian Active Learning (ESB-BAL). Our novelty is to use particle filtering, which is a highly versatile filtering method [10], for posterior computation; and to propose a parallel computing implementation [11, 12] for efficient posterior update and information computation. While previous implementations of active learning either relied on time consuming Monte Carlo (MC) methods [13, 14] or were only applicable to special cases, such as linear models or GLM [7], our proposed solution is fast enough to be used in real-time biological experiments and can be applied to any state-space model.

To illustrate our method, we apply it to the problem of inferring the parameters of a chemical synapse with Short-Term Depression (STD) [15]. The accuracy of these estimates critically depends on the presynaptic stimulation times: if Inter-Stimulation Intervals (ISIs) are longer than the depression time constant, STD will not be precisely quantified. But if the stimulation frequency is too high, the pool of presynaptic vesicles will be depleted, leading to poor parameter estimates [16, 17]. Synaptic characterization is thus a relevant example application for ESB-BAL, but it is also a challenging one: computation needs to be faster than the typical ISI, which can be shorter than a few milliseconds. Using synthetic data, we show that our method allows to significantly reduce the uncertainty of the estimate in comparison to classically used non-adaptive stimulation protocols. We also show that the rate of information gain (in bit/s) of the whole experiment can be optimized by adding a penalty term for longer ISIs. Lastly, we extend active learning to non-myopic designs. Using recordings from acute brain slices from mice, we show that our framework is sufficiently efficient for optimizing not only the immediate next stimulus, but rather the future stimuli in the experiment.

2 Bayesian active learning

When using active learning in sequential experiments, three key elements need to be defined (Figure 1): (1) The **system** to be studied: its parameters θ can be inferred from its observed responses to a set of input stimuli Ψ . Given the stochastic nature of most systems studied in biology, the random variable \mathbf{X} corresponding to the observations can take various values \mathbf{x} according to a distribution $p(\mathbf{x}|\Psi, \theta)$ (see Section 5); (2) A **filter** that computes the posterior distribution of the parameters given the previous inputs and observations $p(\theta|\mathbf{x}, \Psi)$: it is updated after each new observation (see Section 3); (3) A **controller** that computes the next input stimuli so as to maximize a certain utility function (see Section 4). The three following sections will describe each of these elements in detail.

In general, the utility of a given protocol Ψ can be expressed as the mutual information between the parameter random variable Θ and the response random variable \mathbf{X} , i.e. $I_{\Psi}(\Theta; \mathbf{X})$ (see [13, 18] for a detailed discussion). For instance, in synaptic characterization, Ψ corresponds to a set of T stimulation times $\psi_{1:T}$ and observations correspond to recorded excitatory postsynaptic currents

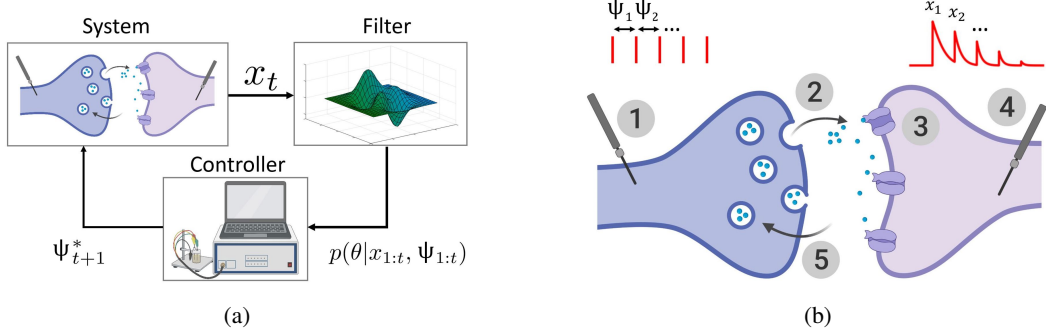


Figure 1: (a) Bayesian active learning applied to synaptic characterization. At each time step, the response of the synapse (**system**) to artificial stimulation is recorded. This observation x_t is used by the **filter** to compute the posterior distribution of parameters $p(\theta|x_{1:t}, \psi_{1:t})$. The **controller** then computes the next stimulation time ψ_{t+1}^* to maximize the expected gain of information. (b) Model of binomial synapse with STD. (1): the presynaptic axon is stimulated. (2): After spike t , k_t vesicles (out of the n_t available ones) release their neurotransmitter with a probability p . (3): A single release event triggers a quantal response q . (4): the total recorded postsynaptic response x_t is the sum of the effects of the k_t release events. (5): After releasing, vesicles are replenished with a time constant τ_D , which determines short-term depression.

(EPSCs) $x_{1:T}$. In case of successive experiments [8], the mutual information between the parameters and the next observation x_{t+1} conditioned on the experiment history $h_t = (x_{1:t}, \psi_{1:t})$ is:

$$I_{h_t}^{\psi_{t+1}}(\Theta; X_{t+1}) = H_{h_t}(\Theta) - H_{h_t}^{\psi_{t+1}}(\Theta|X_{t+1}) \quad (1)$$

where $H_{h_t}(\Theta)$ is the entropy of the distribution of Θ at time t ; and

$$H_{h_t}^{\psi_{t+1}}(\Theta|X_{t+1}) = \int dx_{t+1} p(x_{t+1}|h_t, \psi_{t+1}) H_{h_t}^{\psi_{t+1}}(\Theta|X_{t+1} = x_{t+1})$$

is the conditional entropy of the distribution of Θ at time $t + 1$. The latter depends on the future observation x_{t+1} , which is unknown. We thus take its average over x_{t+1} ; as the predictive distribution depends on the unknown parameters, we also have to take an average over θ , using the current posterior distribution $p(\theta|h_t)$ at time t : $p(x_{t+1}|h_t, \psi_{t+1}) = \int d\theta p(x_{t+1}|h_t, \psi_{t+1}, \theta) p(\theta|h_t)$ [7]. The goal of Bayesian active learning is to select the next stimulation to maximize the mutual information between the parameters and all future observations:

$$\psi_{t+1}^* = \arg \max_{\psi_{t+1}} \max_n \max_{\psi_{t+1:t+n}} I_{h_t}^{\psi_{t+1:t+n}}(\Theta; X_{t+1:t+n}) \quad (2)$$

with $\psi_{t+1:t+n} \in \mathcal{S}_{t+1:t+n}$ where $\mathcal{S}_{t+1:t+n}$ is the set of possible protocols for the next stimulations. Optimizing all future inputs is an intractable problem (especially for online applications), since the algorithmic complexity scales exponentially with the number of observations. For this reason, BAL only optimizes for the next stimulus (an approach referred to as a *myopic* design) (see Figure 1):

$$\psi_{t+1}^* = \arg \max_{\psi_{t+1} \in \mathcal{S}_{t+1}} I_{h_t}^{\psi_{t+1}}(\Theta; X_{t+1}) \quad (3)$$

Different methods have been proposed to compute Eq. 3. Monte Carlo (MC) methods [13] or a variational approach [14] can be employed, but they usually require long computation times that can be impractical if the time between successive experiments is short. Closed-form solutions can be computed for some special cases, such as linear models of GLM [7].

3 The filter: online computation of the posterior distributions of parameters

To be applicable for online experiments, the filtering block (which will compute the posterior distribution of parameters $p(\theta|h_t)$) needs to satisfy two requirements: (1) It must be sufficiently versatile to be applied to different systems and models; (2) It must be online (i.e. its algorithmic complexity should not increase with the number of observations) [19]. A promising solution is particle filtering [20], and especially the Nested Particle Filter (NPF) [10]. This algorithm is asymptotically exact and purely recursive, and thus allows to directly estimate the parameters as recordings are acquired. The NPF relies on two nested layers of particles to approximate the posterior distributions of both the static parameters of the model and of its hidden states. A first outer filter with M_{out} particles is used to compute the posterior distribution of parameters $p(\theta|h_t)$, and for each of these particles, an inner filter with M_{in} particles is used to estimate the corresponding hidden states z_t (so that the total number of particles in the system is $M_{\text{out}} \times M_{\text{in}}$). After each new observation, these particles are resampled based on their respective likelihoods (Figure S1).

The NPF was originally proposed for standard HMMs. Here, we extend it to the more general class of Input-Output Hidden Markov Models (IO-HMMs, also called GLM-HMMs in neuroscience [21]), in which state transition probability at time t depends on an external input ψ_t . For instance, state transition in our model of synapse is not stationary, but depends on the ISI ψ_t (see Section 5). The filter (Algorithm 2, Section A.1) relies on the following approximation to recursively compute the likelihood of each particle. Once the observation x_t has been recorded, the likelihood of particle θ_t^i (with i in $1 \dots M_{\text{out}}$) depends on

$$p(\theta_t^i|x_{1:t}) \propto p(x_t|x_{1:t-1}, \theta_t^i, \psi_t) p(\theta_t^i|x_{1:t-1}) \quad (4)$$

with

$$p(x_t|x_{1:t-1}, \theta_t^i, \psi_t) = \sum_{z_{t-1:t}} p(x_t|z_t, \theta_t^i) p(z_t|z_{t-1}, \theta_t^i, \psi_t) p(z_{t-1}|x_{1:t-1}, \theta_t^i) \quad (5)$$

If the variance of the jittering kernel κ (which mutates the samples to avoid particles degeneracy and local solutions, see Section 3.2 in [10] for a detailed discussion) is sufficiently small, and hence if $\theta_t^i \approx \theta_{t-1}^i$, the approximation $p(z_{t-1}|x_{1:t-1}, \theta_t^i) \approx p(z_{t-1}|x_{1:t-1}, \theta_{t-1}^i)$ allows to recursively compute Eq. 4. In practice, the different terms in Eq. 5 are computed as such: $p(x_t|z_t, \theta_t^i)$ corresponds to the *Likelihood* step of Algorithm 2; $p(z_t|z_{t-1}, \theta_t^i, \psi_t)$ corresponds to the *Propagation* step; and $p(z_{t-1}|x_{1:t-1}, \theta_t^i)$ corresponds to the distribution of hidden states at time $t-1$ (see Section 3.4 in [10] for a detailed explanation).

Contrary to previous methods for fast posterior computation that were only applicable to specific models [7], our filter can be applied to a broad range of state-space dynamical systems, including non-stationary and input-dependent ones. Moreover, it does not require to approximate the posterior as a Gaussian nor require a time consuming (and possibly unstable) numerical optimization step, while being highly parallelizable and efficient [11, 12].

4 The controller: computation of the optimal next stimulation time

The objective of experiment design optimization is to minimize the uncertainty of the estimates (classically quantified using the entropy) while reducing the cost of experimentation (defined as the number of required trials, samples, or observations). The optimal next stimulus ψ_{t+1}^* that will maximize the mutual information (i.e. minimize the uncertainty about θ as measured by the entropy) can be written from Eq. 1 and 3 as

$$\psi_{t+1}^* = \arg \min_{\psi_{t+1} \in \mathcal{S}_{t+1}} \int d\theta p(\theta|h_t) \int dx_{t+1} p(x_{t+1}|h_t, \psi_{t+1}, \theta) H_{h_t}^{\psi_{t+1}}(\Theta|X_{t+1} = x_{t+1}) \quad (6)$$

Eq. 6 requires to compute two (possibly high-dimensional) integrals over θ and x_{t+1} , for which closed-form expressions only exist for specific models. To avoid long MC simulations, we propose to use mean-field computations and to replace integrals by point-based approximations. Firstly, instead

Algorithm 1: Computation of the optimal next stimulation time for synaptic characterization

set $\hat{\theta}_t = \arg \max_{\theta} p(\theta|h_t)$ (MAP values from the current posterior estimation);

Input: \mathcal{S}_{t+1} (set of candidates ψ_{t+1});

for ψ_{t+1} in \mathcal{S}_{t+1} **do**

 | Compute $\mathbb{E}(X_{t+1}|\psi_{1:t+1}, \hat{\theta}_t)$ using Eq. S1;

 | Compute $H_{h_t}^{\psi_{t+1}}(\Theta|X_{t+1} = \mathbb{E}(X_{t+1}|\psi_{1:t+1}, \hat{\theta}_t))$ using Algorithm 2;

end

$$\psi_{t+1}^* = \arg \min_{\psi_{t+1} \in \mathcal{S}_{t+1}} H_{h_t}^{\psi_{t+1}}(\Theta|X_{t+1} = \mathbb{E}(X_{t+1}|\psi_{1:t+1}, \hat{\theta}_t))$$

of computing the full expectation over $p(\theta|h_t)$, we set θ to its maximum a posteriori (MAP) value $\hat{\theta}_t = \arg \max_{\theta} p(\theta|h_t)$. Eq. 6 thus becomes

$$\psi_{t+1}^* \approx \arg \min_{\psi_{t+1} \in \mathcal{S}_{t+1}} \int dx_{t+1} p(x_{t+1}|h_t, \psi_{t+1}, \hat{\theta}_t) H_{h_t}^{\psi_{t+1}}(\Theta|X_{t+1} = x_{t+1})$$

Depending on the nature of the studied system and on the time constraints of the experiment, different estimators can also be used, such as e.g. $\hat{\theta}_t = \frac{1}{M_{\text{out}}} \sum_{i=1}^{M_{\text{out}}} \theta_t^i$. Secondly, instead of computing the full expectation over the future observation, we set x_{t+1} to its expected value; Eq. 6 thus becomes

$$\psi_{t+1}^* \approx \arg \min_{\psi_{t+1} \in \mathcal{S}_{t+1}} H_{h_t}^{\psi_{t+1}}(\Theta|X_{t+1} = \mathbb{E}(X_{t+1}|h_t, \psi_{t+1}, \hat{\theta}_t))$$

In the general case, $\mathbb{E}(X_{t+1}|h_t, \psi_{t+1}, \hat{\theta}_t)$ can be computed using Bayesian Quadrature [22]. More specifically, for our model of a chemical synapse, an analytical formulation for the expected value $\mathbb{E}(X_{t+1}|\psi_{1:t+1}, \hat{\theta}_t)$ can be efficiently derived using mean-field approximations (see Section A.2). For each candidate ψ_{t+1} in a given finite set \mathcal{S}_{t+1} , the entropy $H_{h_t}^{\psi_{t+1}}(\Theta|X_{t+1} = \mathbb{E}(X_{t+1}|h_t, \psi_{t+1}, \hat{\theta}_t))$ can be computed using Algorithm 2. Similarly as in [21], the entropy of the posterior distribution of Θ is approximated as $\frac{1}{2} \log |2\pi e \Sigma_t|$, where Σ_t is the covariance matrix of the particles $\{\theta_t^i\}_{1 \leq i \leq M_{\text{out}}}$.

5 The system: a binomial model of neurotransmitter release

A classically used model to describe the release of neurotransmitters at chemical synapses is called the binomial model [23, 1, 2, 16, 24, 25, 26]. Under this model, a synapse is described as a Input-Output Hidden Markov Model (IO-HMM) with the following parameters (units are given in square brackets, see also Figure 1 (b)): N (the number of independent release sites [-]); p (their release probability [-]); σ (the recording noise [A]); q (the quantum of current elicited by one release event [A]); τ_D (the time constant of synaptic vesicle replenishment [s]). The variables n_t , k_t , and x_t represent, respectively, the number of available vesicles at the moment of spike t , the number of vesicles released after spike t , and the t -th recorded EPSC. For simplicity, we use the notation $p_\theta(\cdot) = p(\cdot|\theta)$ with $\theta = [N, p, q, \sigma, \tau_D]$. The probability of recording $x_{1:T}$ is computed as the marginal of the joint distribution of the observations $x_{1:T}$ and the hidden variables $n_{1:T}$ and $k_{1:T}$:

$$p_\theta(x_{1:T}, n_{1:T}, k_{1:T}) = p_\theta(x_1|k_1) p_\theta(k_1|n_1) p_\theta(n_1) \prod_{t=2}^T p_\theta(x_t|k_t) p_\theta(k_t|n_t) p_\theta(n_t|n_{t-1}, k_{t-1}, \psi_t) \quad (7)$$

where $p_\theta(x_t|k_t) = \mathcal{N}(x_t; qk_t, \sigma^2)$ is the emission probability, i.e. the probability to record x_t knowing that k_t vesicles released neurotransmitter; $p_\theta(k_t|n_t)$ is the binomial distribution and represents the probability that, given n_t available vesicles, k_t of them will indeed release neurotransmitter: $p_\theta(k_t|n_t) = \binom{n_t}{k_t} p^{k_t} (1-p)^{n_t-k_t}$; and $p_\theta(n_t|n_{t-1}, k_{t-1}, \psi_t)$ represents the process of vesicle replenishment. During the time interval ψ_t , each empty vesicle can refill with a probability $I_t(\psi_t) = 1 - \exp\left(-\frac{\psi_t}{\tau_D}\right)$ such that the transition probability $p_\theta(n_t|n_{t-1}, k_{t-1}, \psi_t)$ is given by:

$$p_\theta(n_t|n_{t-1}, k_{t-1}, \psi_t) = \binom{N - n_{t-1} + k_{t-1}}{n_t - n_{t-1} + k_{t-1}} I_t(\psi_t)^{n_t - n_{t-1} + k_{t-1}} (1 - I_t(\psi_t))^{N - n_t} \quad (8)$$

Eqs. 7 to 8 define the observation model of the studied system (see Figure 1), i.e. the probability of an observation x_t given a vector of stimuli $\psi_{1:t}$ and a vector of parameters θ .

6 Results

6.1 First setting: reducing the uncertainty of estimates for a given number of observations

To illustrate our ESB-BAL framework, we apply it to the problem of estimating the parameters of a chemical synapse (Algorithm 1). From the experimentalist point of view, a highly relevant question is how to optimize the stimulation protocol such that the measured EPSCs are most informative about synaptic parameters. Previous studies showed that some stimulation protocols are more informative than others, but ignored the temporal correlations of the number of readily-releasable vesicles [27] or did not compute which protocol would be most informative [1].

Results for a simulated experiment with ground-truth parameters $N^* = 7$, $p^* = 0.6$, $q^* = 1$ pA, $\sigma^* = 0.2$ pA, and $\tau_D^* = 0.25$ s (i.e. the same set of parameters θ^* used in [2]) are displayed in Figure 2 (a). Here, we compare ESB-BAL to 3 deterministic protocols: in the *Constant* protocol, the synapse is probed at a constant frequency, i.e. $\Delta_t = \text{cst}$; in the *Uniform* protocol, ISIs are uniformly drawn from a set \mathcal{S} of candidates ψ_t consisting of equidistantly separated values ranging from $\Delta_t^{\min} = 0.005$ s (i.e. one order of magnitude shorter than the shortest ISI used in [1]) to Δ_t^{\max} , i.e. $\psi_t \sim \mathcal{U}([0.005, \Delta_t^{\max}])$; finally, in the *Exponential* protocol, ISIs are drawn from an exponential distribution with mean τ . The efficiency of these deterministic protocols will depend on their respective parametrizations. To conservatively assess ESB-BAL, we optimize the values of Δ_t , Δ_t^{\max} , and τ so that the *Constant*, *Uniform*, and *Exponential* protocols have the best possible performance for the used ground-truth parameters θ^* . Figure S2 shows the average final entropy decrease (i.e. the information gain) after 200 observations using the *Constant* (top), *Uniform* (middle), or *Exponential* (bottom) protocol, for different values of their hyperparameters. These deterministic protocols (with their optimal respective parametrizations) are then compared to ESB-BAL.

For the different protocols, the average (over 100 independent repetitions) joint differential entropy of the posterior distribution of parameters is plotted as a function of the number of observations. ESB-BAL allows to significantly reduce the uncertainty (as measured by the entropy) of the parameter estimates for a given number of observations. It should be noted that it is compared to deterministic protocols whose respective hyperparameters have been optimized offline, knowing the value of θ^* . In real physiology experiments, classical protocols are non-adaptive and are defined using (possibly sub-optimal) default parameters. In contrast, in active learning the protocol is optimized on the fly as data are recorded, and its performance will not depend on a prior parametrization. ESB-BAL thus outperforms the best possible *Constant*, *Uniform*, and *Exponential* protocols.

We also verify that ESB-BAL does not lead to biased estimates of θ , as its average Root Mean-Squared Error (RMSE) outperforms that of other protocols (Figure 2 (b)); and that it is sufficiently fast for online applications, as computation time exceeds the ISI in only a small proportion of cases (Figure 2 (c)). Similar results can be observed for different sets of ground-truth parameters θ^* (Figure S3) or when only optimizing for the entropy of a specific parameter (Figure S4). Finally, in Figure S5, ESB-BAL (black dashed line) is compared to exact active learning (gray dashed line), in which Eq. 6 is computed exactly using MC samples. Samples to compute the expectation over θ are drawn from $p(\theta|h_t)$, whereas samples used to compute the expectation over x_{t+1} are drawn from a normal distribution with mean $\mathbb{E}(X_{t+1})$ (Eq. S1) and variance $\text{Var}(X_{t+1})$ (Eq. S2). This shows that the approximations used in Algorithm 1 to make active learning online have only a small effect on performance.

6.2 Second setting: reducing the uncertainty of estimates for a given experiment time

Active learning allows, for a given number of observations, to improve the reliability of the estimated parameters. However, in its classical implementation, only the next stimulus input is optimized, disregarding all future observations in the experiment. This myopic approach is thus sub-optimal. Moreover, neurophysiology experiments are not only constrained by the number of observations, but also by the total time of the experiment. Since cell viability and recording stability may become limiting during an experiment, the total time of an experimental protocol $\sum_{t=1}^T \psi_t$ also needs to be accounted for. Here, to account for the total time of the experiment, and to globally optimize the

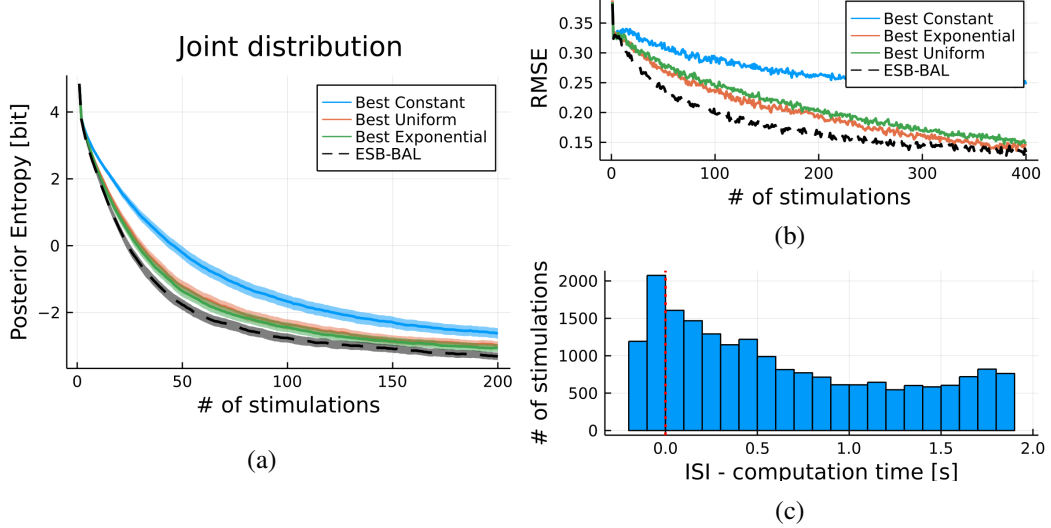


Figure 2: **First setting: reducing the uncertainty of estimates for a given number of observations.** (a) Entropy of the posterior distribution of θ vs. number of observations for different stimulation protocols. Synthetic data were generated from a model of synapse with ground truth parameters $N^* = 7$, $p^* = 0.6$, $q^* = 1$ A, $\sigma^* = 0.2$ A, and $\tau_D^* = 0.25$ s [2]. Traces show average over 100 independent repetitions. Shaded area: standard error of the mean. (b) RMSE for the same simulations. (c) Histogram of the differences between the ISI and the corresponding computation time for the ESB-BAL simulations.

information gain per unit of time, we propose to modify the classical formulation of active learning (Eq. 6) by adding a penalty term for longer ISIs:

$$\psi_{t+1}^{*(\eta)} = \arg \min_{\psi_{t+1}} \left\{ \eta \psi_{t+1} + \int d\theta p(\theta|h_t) \int dx_{t+1} p(x_{t+1}|\psi_{1:t+1}, \theta) H_{h_t}^{\psi_{t+1}}(\Theta|x_{t+1}) \right\} \quad (9)$$

The effect of the penalty weight η on the entropy of the posterior distribution of τ_D is displayed in Figure 3 (a). As expected, adding a penalty term to Eq. 6 reduces the precision of the inferred parameter. The loss of information gain increases with the penalty weight η . However, increasing η also increases the speed of information gain, as seen in Figure 3 (b). Depending on the available time for the experiment, it is thus possible to tune η so as to find a trade-off between long-term precision (Figure 3 (a)) and information rate (Figure 3 (b)).

6.3 Third setting: batch optimization and application to neural recordings

To reduce computational complexity, classical implementations of sequential experiment design usually only optimize for the immediate next observation. However, it might be critical for some systems to optimize not only the next stimulus, but rather the next n stimuli of the experiment altogether (see Eq. 2) [6, 28]. Synaptic characterization is a telling example: indeed, STD can only be observed for specifically organized batches of stimulation times. When probing the presynaptic cell, neuroscientists usually use repetitions of a spike train (Figure 4 (b)) consisting of a tetanic stimulation phase (sustained high-frequency stimulation used to deplete the presynaptic vesicles, between 0.1s and 0.3s in Figure 4 (b)) followed by recovery spikes at increasing ISIs to probe the STD time constant [29]. These spike trains are usually not optimized, and are held constant throughout an entire experiment.

Here, we show that ESB-BAL can be used to extend active learning to non-myopic designs, and to optimize the n next input stimuli. Algorithm 3 (Section A.4), which is a generalization of Algorithm 1, is used to select the next batch of n stimuli $\psi_{t+1:t+n}^*$ in a set of candidate batches $\mathcal{S}_{t+1:t+n}$. Every n observations, $H_{h_t}^{\psi_{t+1:t+n}}(\Theta|X_{t+1:t+n})$ is computed using n iterations of the filter (i.e. Algorithm 2), so as to pick the optimal next batch $\psi_{t+1:t+n}^*$ that minimizes this quantity:

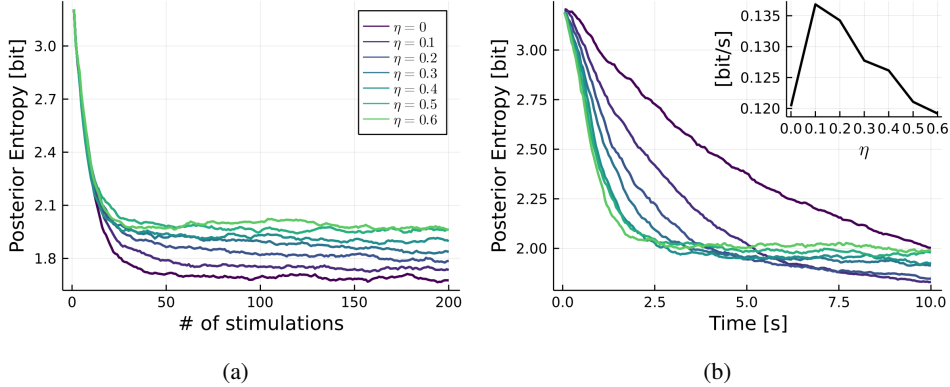


Figure 3: **Second setting: reducing the uncertainty of estimates for a given experiment time** (effect of penalizing long ISIs on parameter estimates uncertainty and rate of information gain). (a) Entropy of the posterior distribution of τ_D vs. number of observations for different values of η in Eq. 9. Same settings as in Figure S3. (b) Same results, but displayed as a function of time. Inset: slope of the entropy vs. time curves (i.e. information rate) vs. η after 10 seconds.

$$\psi_{t+1:t+n}^* = \arg \min_{\psi_{t+1:t+n} \in \mathcal{S}_{t+1:t+n}} H_{h_t}^{\psi_{t+1:t+n}}(\Theta | X_{t+1:t+n})$$

where the next stimulation times in $\mathcal{S}_{t+1:t+n}$ are parametrized with a low-dimensional parametrization so as to span different durations and frequencies for the tetanic phase, and different ISIs between the recovery spikes (see Figure S6).

We validate our method by applying it to EPSC recordings from acute mouse cerebellar slices. Figure 4 (a) shows the marginal posterior distributions for parameters of a cerebellar mossy fiber to granule cell synapse, obtained using either ESB-BAL or a deterministic protocol (consisting of repetitions of the same train of 100 stimuli at 100Hz followed by 6 recovery spikes). In Figure 4 (c), using simulated experiments, we also compare ESB-BAL to an Exponential stimulation protocol (in which ISIs are drawn from an exponential distribution, whose time constant is optimized as in Section 6.1), which has been proposed to provide better estimates of synaptic parameters as it spans a broader frequency space [27]. Our results show that batch optimization via ESB-BAL clearly outperforms deterministic stimulation.

7 Discussion

When designing an experiment in physiology, or when training a model on data in machine learning, it is common to choose a priori a fixed set of inputs to the studied system. The use of such non-adaptive, non-optimized protocols often leads to a large variance of the estimated parameters, even when using a large number of trials or data points. Bayesian active learning is an efficient method for optimizing these inputs, but exact solutions are often intractable and not applicable to online experiments. Here, we introduce ESB-BAL, a novel framework combining particle filtering, parallel computing, and mean-field theory. ESB-BAL is general and sufficiently efficient to be applied to a wide range of settings. We use it to infer the parameters of a model of synapse: for this specific example, computation time is a critical constraint, since the typical ISI is shorter than 1s, and because several future inputs need to be optimized together. Using synthetic data and neural recordings, we show that our method has the potential to significantly improve the precision and speed of model-based inferences.

We expect active learning to be particularly beneficial to neurophysiology experiments involving live cells or subjects. By reducing the number of samples required to obtain a certain result, or by improving the efficiency of information gain, we can reduce the cost of the experiment and the need for animal subjects. A possible negative impact would be that improving the relative efficiency of neurophysiology experiments may lead to a larger field of applications and therefore a larger demand for animal experiments, analogously to Jevons Paradox [30].

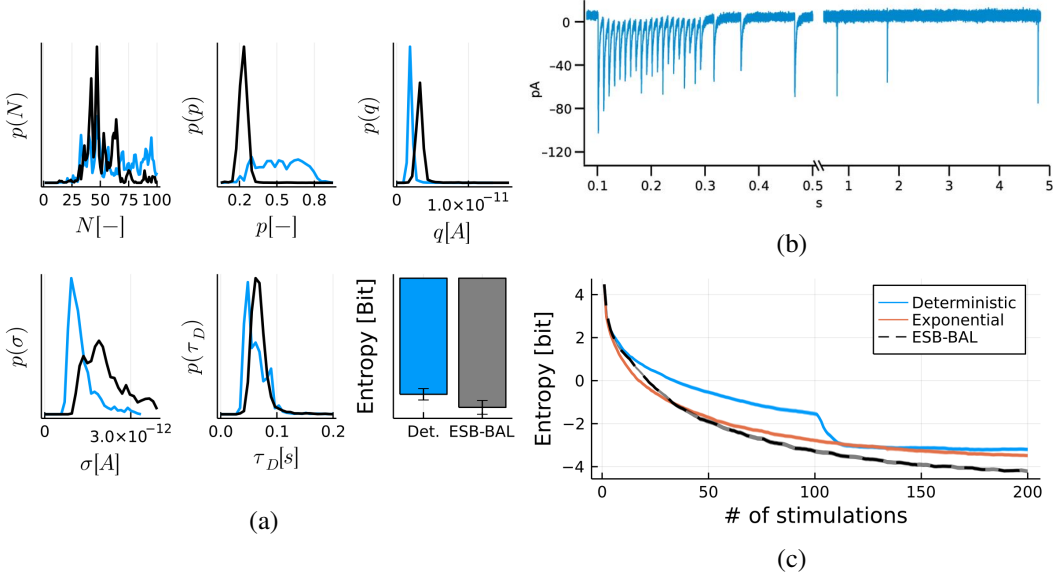


Figure 4: **Third setting: batch optimization and application to neural recordings.** (a) Marginal posterior distributions obtained after 200 stimulations of the same synapse using either the deterministic protocol (blue) or ESB-BAL (black). Posteriors were computed using the Metropolis-Hastings algorithm (50.000 samples). The bar plot indicates the mean differential entropy after 200 observations for 5 recording sessions using the deterministic protocol and 3 recording sessions using ESB-BAL on different synapses. Error bars show the standard error of the mean. Data from cerebellar mossy fiber to granule cell synapses. (b) Example of a postsynaptic current trace recorded using a tetanic stimulation phase followed by 6 recovery spikes. (c) Simulated experiment with ground-truth parameters $N^* = 55$, $p^* = 0.174$, $q^* = 4.86$ pA, $\sigma^* = 1.67$ pA, and $\tau_D^* = 0.0828$ s (i.e. the MAP values from recordings shown in (a)).

Our approach has some room for improvements. An evident drawback of using particle filtering is that it requires a very large number of particles to provide low variance estimates, as the approximation error only decreases with the square root of the number of particles. Moreover, future experimental work should focus on implementing ESB-BAL for different and more complicated models of a chemical synapse, including for instance short-term facilitation [1, 2, 16, 27] or vesicle content variability [31, 32]. Finally, future theoretical work should focus on obtaining results on the convergence of the estimators when using active learning. When observations are independent and identically distributed (i.i.d.), active learning will give an unbiased estimate of the parameters, whose variance will decrease with the number of observations [33]. Such theoretical results lack for systems with correlated outputs (such as the EPSCs in the studied synapse model), possibly leading to information saturation [34] or biased estimates.

Overall, we expect our proposed solution to pave the way towards better estimates of stochastic models in neuroscience, more efficient training in machine learning, and more systematic and automated experimental designs. Especially, applying it to synaptic characterization would allow to better understand the role of synaptic transmission in learning and memory [35], to study the role of synaptic stochasticity [36, 37], and lead to an improved understanding of spike timing-dependent plasticity [38], synaptic homeostasis [39, 40], plasticity [41, 42, 43], and connectivity [44].

Acknowledgments and Disclosure of Funding

The work presented in this paper was supported by the Swiss National Science Foundation under grant number 31003A_175644 entitled "Bayesian Synapse".

Figures were created using BioRender. Calculations were performed on UBELIX (<http://www.id.unibe.ch/hpc>), the HPC cluster at the University of Bern. The CUDA.jl package [11, 12] is licensed under the MIT "Expat" License (<https://github.com/JuliaGPU/CUDA.jl/blob/>

master/LICENSE.md). We thank Ehsan Abedi, Jakob Jordan, and Anna Kutschireiter for the fruitful discussions.

JULIA files are available in the following package: <https://github.com/Theoretical-Neuroscience-Group/BinomialSynapses.jl>

References

- [1] Alessandro Barri, Yun Wang, David Hansel, and Gianluigi Mongillo. Quantifying repetitive transmission at chemical synapses: a generative-model approach. *Eneuro*, 3(2), 2016.
- [2] Alex D Bird, Mark J Wall, and Magnus JE Richardson. Bayesian inference of synaptic quantal parameters from correlated vesicle release. *Frontiers in computational neuroscience*, 10:116, 2016.
- [3] Timo Flesch, Jan Balaguer, Ronald Dekker, Hamed Nili, and Christopher Summerfield. Comparing continual task learning in minds and machines. *Proceedings of the National Academy of Sciences*, 115(44):E10313–E10322, 2018.
- [4] Ashley F Emery and Aleksey V Nenarokomov. Optimal experiment design. *Measurement Science and Technology*, 9(6):864, 1998.
- [5] Paola Sebastiani and Henry P Wynn. Maximum entropy sampling and optimal bayesian experimental design. *Journal of the Royal Statistical Society: Series B (Statistical Methodology)*, 62(1):145–157, 2000.
- [6] Elizabeth G Ryan, Christopher C Drovandi, James M McGree, and Anthony N Pettitt. A review of modern computational algorithms for bayesian optimal design. *International Statistical Review*, 84(1):128–154, 2016.
- [7] Jeremy Lewi, Robert Butera, and Liam Paninski. Sequential optimal design of neurophysiology experiments. *Neural computation*, 21(3):619–687, 2009.
- [8] Mijung Park and Jonathan Pillow. Bayesian active learning with localized priors for fast receptive field characterization. *Advances in neural information processing systems*, 25:2348–2356, 2012.
- [9] Mijung Park, Greg Horwitz, and Jonathan W Pillow. Active learning of neural response functions with gaussian processes. In *NIPS*, pages 2043–2051. Citeseer, 2011.
- [10] Dan Crisan, Joaquin Miguez, et al. Nested particle filters for online parameter estimation in discrete-time state-space markov models. *Bernoulli*, 24(4A):3039–3086, 2018.
- [11] Tim Besard, Christophe Foket, and Bjorn De Sutter. Effective extensible programming: Unleashing Julia on GPUs. *IEEE Transactions on Parallel and Distributed Systems*, 2018.
- [12] Tim Besard, Valentin Churavy, Alan Edelman, and Bjorn De Sutter. Rapid software prototyping for heterogeneous and distributed platforms. *Advances in Engineering Software*, 132:29–46, 2019.
- [13] Xun Huan and Youssef M Marzouk. Simulation-based optimal bayesian experimental design for nonlinear systems. *Journal of Computational Physics*, 232(1):288–317, 2013.
- [14] Adam Foster, Martin Jankowiak, Eli Bingham, Paul Horsfall, Yee Whye Teh, Tom Rainforth, and Noah Goodman. Variational bayesian optimal experimental design. *arXiv preprint arXiv:1903.05480*, 2019.
- [15] J Del Castillo and B3 Katz. Quantal components of the end-plate potential. *The Journal of physiology*, 124(3):560–573, 1954.
- [16] Camille Gontier and Jean-Pascal Pfister. Identifiability of a binomial synapse. *Frontiers in computational neuroscience*, 14:86, 2020.
- [17] Franz-Georg Wieland, Adrian L Hauber, Marcus Rosenblatt, Christian Tönsing, and Jens Timmer. On structural and practical identifiability. *Current Opinion in Systems Biology*, 2021.
- [18] Dennis V Lindley. On a measure of the information provided by an experiment. *The Annals of Mathematical Statistics*, pages 986–1005, 1956.
- [19] Ola Bykowska, Camille Gontier, Anne-Lene Sax, David W Jia, Milton Llera Montero, Alex D Bird, Conor Houghton, Jean-Pascal Pfister, and Rui Ponte Costa. Model-based inference of synaptic transmission. *Frontiers in synaptic neuroscience*, 11:21, 2019.

[20] Anna Kutschireiter, Simone Carlo Surace, and Jean-Pascal Pfister. The hitchhiker's guide to nonlinear filtering. *Journal of Mathematical Psychology*, 94:102307, 2020.

[21] Aditi Jha, Zoe C Ashwood, and Jonathan W Pillow. Bayesian active learning for discrete latent variable models. *arXiv preprint arXiv:2202.13426*, 2022.

[22] Luigi Acerbi. Variational bayesian monte carlo. *Advances in Neural Information Processing Systems*, 31, 2018.

[23] Bernard Katz. The release of neural transmitter substances. *Liverpool University Press*, pages 5–39, 1969.

[24] Christian Stricker and Stephen J Redman. Quantal analysis based on density estimation. *Journal of neuroscience methods*, 130(2):159–171, 2003.

[25] Volker Scheuss and Erwin Neher. Estimating synaptic parameters from mean, variance, and covariance in trains of synaptic responses. *Biophysical journal*, 81(4):1970–1989, 2001.

[26] Misha Tsodyks, Klaus Pawelzik, and Henry Markram. Neural networks with dynamic synapses. *Neural computation*, 10(4):821–835, 1998.

[27] Rui P Costa, P Jesper Sjöström, and Mark CW Van Rossum. Probabilistic inference of short-term synaptic plasticity in neocortical microcircuits. *Frontiers in computational neuroscience*, 7:75, 2013.

[28] Christopher C Drovandi, Minh-Ngoc Tran, et al. Improving the efficiency of fully bayesian optimal design of experiments using randomised quasi-monte carlo. *Bayesian Analysis*, 13(1):139–162, 2018.

[29] Henry Markram, Dimitri Pukas, Anirudh Gupta, and Misha Tsodyks. Potential for multiple mechanisms, phenomena and algorithms for synaptic plasticity at single synapses. *Neuropharmacology*, 37(4-5):489–500, 1998.

[30] William Stanley Jevons. The coal question. *An Inquiry Concerning the Prog*, 1862.

[31] Gardave Singh Bhumbra and Marco Beato. Reliable evaluation of the quantal determinants of synaptic efficacy using bayesian analysis. *Journal of neurophysiology*, 109(2):603–620, 2013.

[32] Cary Soares, Daniel Trotter, André Longtin, Jean-Claude Béïque, and Richard Naud. Parsing out the variability of transmission at central synapses using optical quantal analysis. *Frontiers in synaptic neuroscience*, 11:22, 2019.

[33] Liam Paninski. Asymptotic theory of information-theoretic experimental design. *Neural Computation*, 17(7):1480–1507, 2005.

[34] Rubén Moreno-Bote, Jeffrey Beck, Ingmar Kanitscheider, Xaq Pitkow, Peter Latham, and Alexandre Pouget. Information-limiting correlations. *Nature neuroscience*, 17(10):1410–1417, 2014.

[35] Laurence Aitchison, Jannes Jegminat, Jorge Aurelio Menendez, Jean-Pascal Pfister, Alexandre Pouget, and Peter E Latham. Synaptic plasticity as bayesian inference. *Nature Neuroscience*, 24(4):565–571, 2021.

[36] William B Levy and Robert A Baxter. Energy-efficient neuronal computation via quantal synaptic failures. *Journal of Neuroscience*, 22(11):4746–4755, 2002.

[37] Daqing Guo and Chenguang Li. Stochastic resonance in hodgkin–huxley neuron induced by unreliable synaptic transmission. *Journal of theoretical biology*, 308:105–114, 2012.

[38] Jean-Pascal Pfister and Wulfram Gerstner. Triplets of spikes in a model of spike timing-dependent plasticity. *Journal of Neuroscience*, 26(38):9673–9682, 2006.

[39] Graeme W Davis and Martin Müller. Homeostatic control of presynaptic neurotransmitter release. *Annual review of physiology*, 77:251–270, 2015.

[40] Corinna Wentzel, Igor Delvendahl, Sebastian Sydlik, Oleg Georgiev, and Martin Müller. Dysbindin links presynaptic proteasome function to homeostatic recruitment of low release probability vesicles. *Nature communications*, 9(1):1–16, 2018.

[41] Rui Ponte Costa, Robert C Froemke, P Jesper Sjöström, and Mark CW van Rossum. Correction: Unified pre-and postsynaptic long-term plasticity enables reliable and flexible learning. *Elife*, 4:e11988, 2015.

[42] Rui Ponte Costa, Beatriz EP Mizusaki, P Jesper Sjöström, and Mark CW van Rossum. Functional consequences of pre-and postsynaptic expression of synaptic plasticity. *Philosophical Transactions of the Royal Society B: Biological Sciences*, 372(1715):20160153, 2017.

[43] Rui Ponte Costa, Zahid Padamsey, James A D’Amour, Nigel J Emptage, Robert C Froemke, and Tim P Vogels. Synaptic transmission optimization predicts expression loci of long-term plasticity. *Neuron*, 96(1):177–189, 2017.

[44] Luke Campagnola, Stephanie C Seeman, Thomas Chartrand, Lisa Kim, Alex Hoggarth, Clare Gamlin, Shinya Ito, Jessica Trinh, Pasha Davoudian, Cristina Radaelli, et al. Connectivity and synaptic physiology in the mouse and human neocortex. *bioRxiv*, 2021.

A Appendix

A.1 Particle Filtering for synaptic characterization

Algorithm 2: Particle filtering [10] for computing one step update of the posterior distribution of parameters

Input: $\{\theta_{t-1}^i\}_{1 \leq i \leq M_{\text{out}}}$, $\{n_{t-1}^{i,j}, k_{t-1}^{i,j}\}_{1 \leq j \leq M_{\text{in}}}$, x_t, ψ_t ;
for i in $1 \dots M_{\text{out}}$ **do**

Jittering: update the outer particles $\theta_t^i = \kappa(\theta_{t-1}^i)$;

for j in $1 \dots M_{\text{in}}$ **do**

Propagation: Draw $n_t^{i,j} \sim p(n_t^{i,j} | n_{t-1}^{i,j}, k_{t-1}^{i,j}, \theta_t^i, \psi_t)$ and $k_t^{i,j} \sim p(k_t^{i,j} | n_t^{i,j}, \theta_t^i)$;

Likelihood: compute $\tilde{w}_t^{i,j} = p(x_t | n_t^{i,j}, k_t^{i,j}, \theta_t^i)$;

end

Normalization: $\tilde{w}_t^{i,j} \leftarrow \tilde{w}_t^{i,j} / \sum_j \tilde{w}_t^{i,j}$;

Inner particles resampling: resample $\{n_t^{i,j}, k_t^{i,j}\}_{1 \leq j \leq M_{\text{in}}}$ based on $\{\tilde{w}_t^{i,j}\}_{1 \leq j \leq M_{\text{in}}}$;

end

Compute $w_t^i = \frac{1}{M_{\text{in}}} \sum_j \tilde{w}_t^{i,j}$;

Normalization: $w_t^i \leftarrow w_t^i / \sum_i w_t^i$;

Outer particles resampling: resample $\{\theta_t^i\}_{1 \leq i \leq M_{\text{out}}}$ and $\{n_t^{i,j}, k_t^{i,j}\}_{1 \leq j \leq M_{\text{in}}}$ based on $\{w_t^i\}_{1 \leq i \leq M_{\text{out}}}$;

Output: $\{\theta_t^i\}_{1 \leq i \leq M_{\text{out}}}$, $\{n_t^{i,j}, k_t^{i,j}\}_{1 \leq j \leq M_{\text{in}}}$

Computing the posterior distribution of θ also implies to specify a prior $p(\theta)$ from which the initial particles $\{\theta_0^i\}_{1 \leq i \leq M_{\text{out}}}$ will be drawn. For simplicity, we consider here uniform priors (as in [2, 16]), although the algorithm readily extends to different choices of prior.

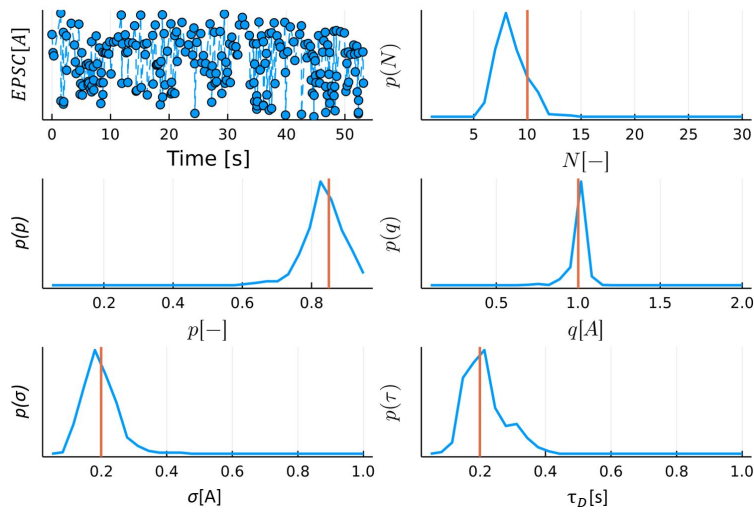


Figure S1: Examples of posteriors obtained using the filter (Algorithm 2). Upper left panel: train of synthetic EPSCs generated from the model described in Section 5. Other panels: posterior distributions of the parameters after 230 stimulations. Ground-truth values used to generate the EPSCs are displayed as red vertical lines.

A.2 Mean-field approximation of vesicle dynamics

Our synapse model, as defined by Eq. 7 to 8, is a Hidden Markov Model with observations x_t and hidden states n_t and k_t . The predictive distribution $p(x_{t+1}|x_{1:t}, \psi_{1:t+1}, \theta)$ used in Eq. 1 can be computed using the Baum-Welch algorithm: however, the algorithmic complexity of this forward-backward procedure, which scales with N^4 , makes it impractical for closed-loop applications. Here, we suggest that computation can be massively simplified by using a mean-field approximation of vesicle dynamics: the analytical mean and variance of hidden and observed variables can be computed using recursive formulæ.

Let $r_t \in [0, 1]$ denote the average fraction of release-competent vesicles at the moment of spike t . Its values, given $\theta = [N, p, q, \sigma, \tau_D]$ and $\psi_{1:t}$, can be iteratively computed (see [1], Eq. (7)) from the equations of the Tsodyks-Markram model [26]: $r_t = 1 - (1 - (1 - p)r_{t-1}) \exp\left(-\frac{\psi_t}{\tau_D}\right)$ with $r_1 = 1$. It follows that the expected value of the EPSC after spike t is

$$\mathbb{E}(X_t|\psi_{1:t}, \theta) = r_t N p q \quad (\text{S1})$$

Similarly, the variance of the number of available vesicles $\text{Var}(n_t)$ can be computed using the law of total variance: $\text{Var}(n_t) = \mathbb{E}(\text{Var}(n_t|n_{t-1}, k_{t-1})) + \text{Var}(\mathbb{E}(n_t|n_{t-1}, k_{t-1}))$. Since $n_t = n_{t-1} - k_{t-1} + v_t$ with $v_t \sim \text{Bin}(N - n_{t-1} + k_{t-1}, I_t)$, it follows that $\text{Var}(n_t) = I_t(1 - I_t)N(1 - r_{t-1} + p r_{t-1}) + (1 - I_t)^2 \text{Var}(n_{t-1} - k_{t-1})$.

Finally, by noting that $(n_t - k_t)|n_t \sim \text{Bin}(n_t, 1 - p)$ and using again the law of total variance to compute $\text{Var}(n_{t-1} - k_{t-1}) = \mathbb{E}(\text{Var}(n_{t-1} - k_{t-1}|n_{t-1})) + \text{Var}(\mathbb{E}(n_{t-1} - k_{t-1}|n_{t-1}))$, we obtain

$$\text{Var}(X_t|\psi_{1:t}, \theta) = \sigma^2 + q^2(N r_t p (1 - p) + \text{Var}(n_t) p^2) \quad (\text{S2})$$

A.3 First setting: reducing the uncertainty of estimates for a given number of observations

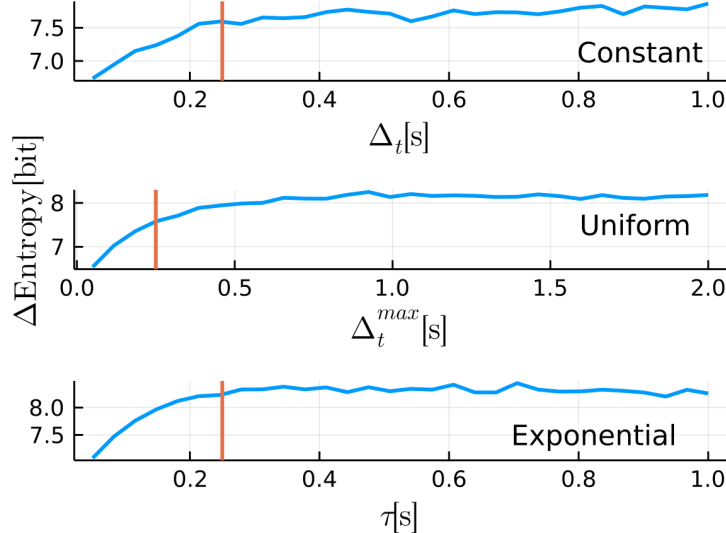


Figure S2: Average final entropy decrease (i.e. information gain) after 200 observations using the *Constant* (top), *Uniform* (middle), or *Exponential* (bottom) protocol, for different values of their hyperparameters. Ground truth parameters used are $N^* = 7$, $p^* = 0.6$, $q^* = 1 \text{ A}$, $\sigma^* = 0.2 \text{ A}$, and $\tau_D^* = 0.25 \text{ s}$ [2]. Vertical red lines indicate the ground truth value $\tau_D^* = 0.25 \text{ s}$ used for simulations. Optimal values for Δ_t , Δ_t^{\max} , and τ are used in Figure 2.

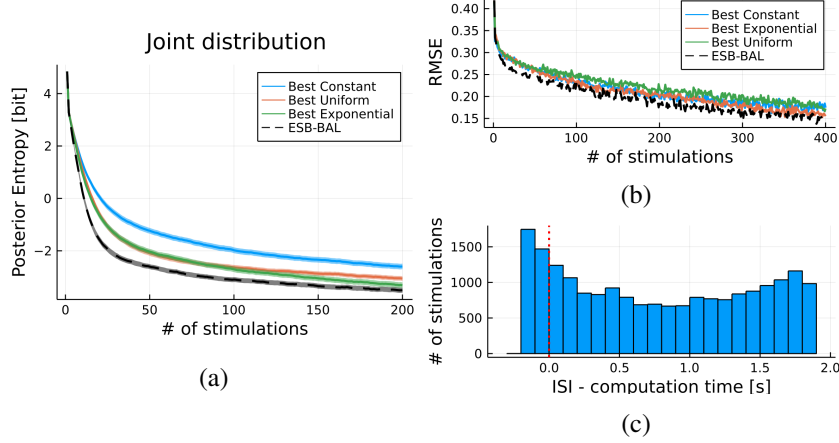


Figure S3: Same setting as in Figure 2 but for ground truth parameters $N^* = 10$, $p^* = 0.85$, $q^* = 1$ A, $\sigma^* = 0.2$ A, and $\tau_D^* = 0.2$ s.

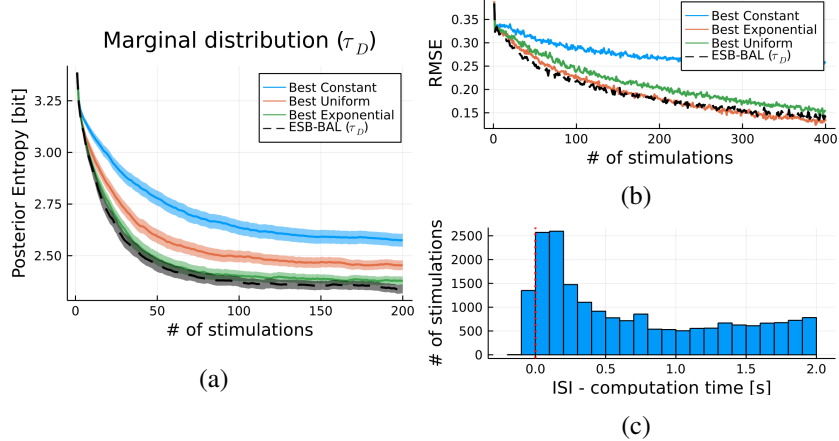


Figure S4: Same setting as in Figure 2 but when optimizing solely for the marginal posterior distribution of τ_D .

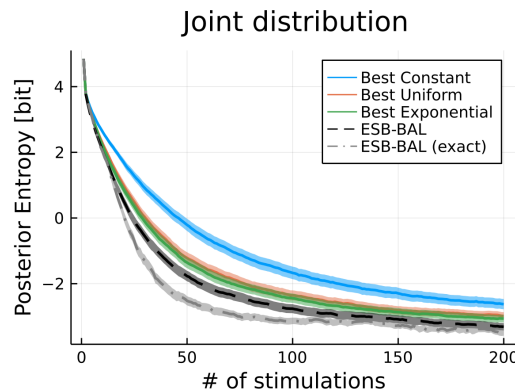


Figure S5: Same setting as in Figure 2, but with exact active learning (gray dashed line), in which Eq. 6 is computed exactly using MC samples.

A.4 Third setting: batch optimization and application to neural recordings

Algorithm 3: Computation of the optimal next batch of ISIs

set $\hat{\theta}_t = \arg \max_{\theta} p(\theta|h_t)$ (MAP values from the current posterior estimation);

Input: $\mathcal{S}_{t+1:t+n}$ (set of candidates $\psi_{t+1:t+n}$);

for $\psi_{t+1:t+n}$ in $\mathcal{S}_{t+1:t+n}$ **do**

 | Compute $H_{h_t}^{\psi_{t+1:t+n}}(\Theta|X_{t+1:t+n})$ using Algorithm 2;

end

$\psi_{t+1:t+n}^* = \arg \min_{\psi_{t+1:t+n} \in \mathcal{S}_{t+1:t+n}} H_{h_t}^{\psi_{t+1:t+n}}(\Theta|X_{t+1:t+n})$

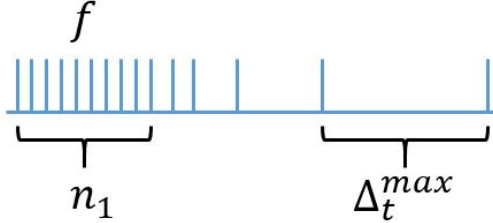


Figure S6: Schematic of how elements in $\mathcal{S}_{t+1:t+n}$ in Algorithm 3 are defined. Assuming that each element in $\mathcal{S}_{t+1:t+n}$ contains n ISIs, they are chosen so as to span 3 parameters: the number $n_1 < n$ of spikes in the tetanic stimulation phase, the frequency f of spikes in the tetanic stimulation phase, and the duration of the final recovery ISI Δ_t^{max} . The remaining $n_1 - 2$ spikes are then distributed geometrically between the end of the tetanic phase and the enultimate spike.